Counting Statistics for Electron Capture in a Dynamic Quantum Dot

Lukas Fricke,[1] Michael Wulf,[1] Bernd Kaestner,[1,*] Vyacheslavs Kashcheyevs,[2,3] Janis Timoshenko,[2,3] Pavel Nazarov,[2,3] Frank Hohls,[1] Philipp Mirovsky,[1] Brigitte Mackrodt,[1] Ralf Dolata,[1] Thomas Weimann,[1] Klaus Pierz,[1] and Hans W. Schumacher[1]

[1]*Physikalisch-Technische Bundesanstalt, Bundesallee 100, 38116 Braunschweig, Germany*
[2]*Faculty of Computing, University of Latvia, Riga LV-1586, Latvia*
[3]*Faculty of Physics and Mathematics, University of Latvia, Riga LV-1002, Latvia*

(Received 8 November 2012; published 20 March 2013)

We report noninvasive single-charge detection of the full probability distribution P_n of the initialization of a quantum dot with n electrons for rapid decoupling from an electron reservoir. We analyze the data in the context of a model for sequential tunneling pinch-off, which has generic solutions corresponding to two opposing mechanisms. One limit considers sequential ''freeze-out'' of an adiabatically evolving grand canonical distribution, the other one is an athermal limit equivalent to the solution of a generalized decay cascade model. We identify the athermal capturing mechanism in our sample, testifying to the high precision of our combined theoretical and experimental methods. The distinction between the capturing mechanisms allows us to derive efficient experimental strategies for improving the initialization.

DOI: 10.1103/PhysRevLett.110.126803 PACS numbers: 73.23.−b, 73.22.Dj, 73.63.Kv

The fast formation of quantum dots (QDs) out of a two-dimensional electron system (2DES) constitutes an open problem within the field of nanoscale electronics [1]. A highly reliable initialization of such *dynamic* QDs is a key ingredient in devices for quantum information processing [2,3], nanoelectronics [4,5], or single-electron current sources [6–8]. The latter device type has been considered as a potential primary measurement standard of electrical current within a modernized international system of units (SI) [9,10]. As dynamic QDs constitute one of the most promising single-electron sources [8], understanding the capturing process will be of broad fundamental and technological interest.

The outcome of the initialization is characterized by a probability distribution P_n for trapping exactly n electrons in the QD. At high repetition rate deviations from a low-dispersion distribution may be caused, e.g., by backtunneling [11–13] or nonadiabatic excitations [14–16]. A decay cascade model [13] has been proposed recently to predict P_n in dynamic QDs. It has become popular for benchmarking QD-based current sources [17–20], which transfer electrons through dynamic QDs at a sufficiently high repetition rate. Alternative mechanisms, such as sudden decoupling from thermal equilibrium [21] have been proposed. Experimental distinction between the capturing mechanisms is the key towards systematic improvement of the initialization precision. So far P_n has not been measured with sufficient accuracy to allow this distinction. The first two cumulants of P_n have been extracted from current and noise measurements [22–24]. Furthermore, single charge detection [21,25] has been used to determine partial information on the distribution of QD population-depopulation events.

Here we present noninvasive charge detection to measure the full probability distribution P_n. Considering the integer charge on the QD to be the only degree of freedom out of equilibrium, we derive theoretically two generic limits for P_n: a (generalized) frozen grand canonical distribution and a rate-driven athermal limit (generalizing the decay cascade model [13]). Both limits may be hard to distinguish experimentally for $P_n \approx 1$, which is the relevant regime for most applications. Yet, our experimental data for P_n allow us to distinguish the two limits and to conclude that the dynamic QD initialization is consistent with the athermal distribution. Based on these findings, strategies for optimum high fidelity initialization are presented.

The device under investigation is shown in Fig. 1(a), with four QD structures in series consisting each of three gates crossing a 2DES within a AlGaAs/GaAs heterostructure. The 2DES is located 90 nm below the surface, the wet-etched channel is 800 nm wide. Similar QD structures have previously been used as single-electron current sources [7,26]. We use the left QD as the dynamic QD, which captures electrons from source (S) and afterwards emits them to the *node* (dotted region) for charge detection. The voltage on one gate of the rightmost QD, V_{barrier}, controls the transparency of the node to the drain lead (D). All other gates are grounded and do not affect the circuit. Close to the node two single-electron transistors (SET) based on Al-AlO_x-Al tunnel junctions are placed as charge detectors (Det1 or Det2). They are operated at fixed voltage bias, using the current as detector signal. To increase the coupling between the potential of the node and the metallic detectors both are capacitively coupled by H-shaped floating gates. Correlating the detector signals allows us to distinguish the electron signal from background charge fluctuations, as both detectors are coupled to the same island. All measurements are performed in a dry dilution cryostat at nominal temperature of about 25 mK.

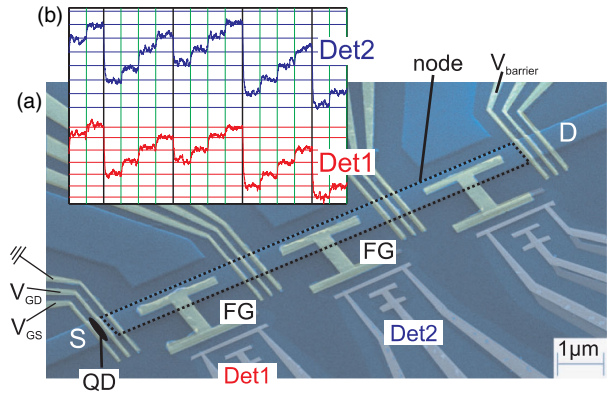

FIG. 1 (color online). (a) False-color electron microscopy image of a device. The upper half shows the semiconducting part consisting of an 800-nm wide channel (light blue) crossed by top gates (yellow). The QD is formed by the leftmost group of top gates, between source (S) and drain (D). The light-gray parts in the lower part form the SETs labeled Det1 (red) and Det2 (blue), respectively. FG labels the floating gates coupling the detectors to the channel. (b) Detector signals of the charge transfer sequence, as explained in the main text.

Figure 2(a) shows the sequence of QD initialization and charge transfer to the node schematically. An isolated QD (ii) is formed between the two leftmost gates by applying sufficiently negative dc voltages, V_{GS} and V_{GD} (see Fig. 1). Initialization (i) of the QD is achieved by applying the first half cycle of a sinusoidal pulse superimposed onto the source gate, so that the source barrier becomes transparent. During the subsequent rise of the source barrier a certain charge state of the isolated QD (ii) with n electrons is established with probability P_n. In the second half cycle of the sinusoidal pulse (iii) the left barrier is raised further. As the source barrier also couples to the QD potential, i.e., acts as plunger gate [26], one can ensure complete unloading of the QD charge to the node where it can be detected noninvasively.

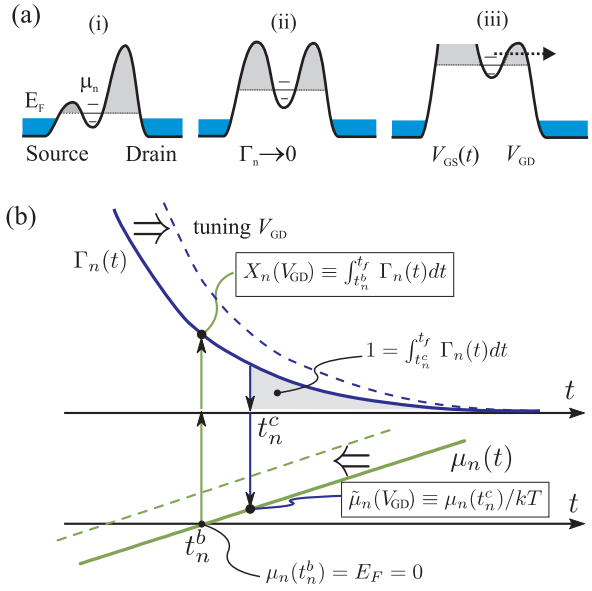

FIG. 2 (color online). (a) Sequence of schematic potential landscapes during capturing from source (i), isolation (ii), and emission to drain (iii), respectively. Shading indicates tunneling rates Γ_n, related to the area under the curve. (b) Evolution of the tunneling rate Γ_n and energy μ_n of a particular charge state for two different V_{GD} voltage settings.

The cycle is repeated three times during which charges accumulate on the node. Afterwards, opening the right barrier resets the node charge, before the next three cycles start. Example traces of the SET signals are shown in Fig. 1(b). The bold black vertical lines represent resets of the node's charge state. The stochastic nature of this process is represented by the different initial states after each reset. Each thin green vertical line represents a combined charge capture and transfer pulse. Because of the discreteness of node charges, we can assign levels (horizontal lines) derived from a histogram of the detector trace to each interval between pulses. These are then compared to extract the number of captured electrons in this specific cycle [27]. Because of the limited bandwidth of the SET detectors ($f_{bw} \approx 600$ Hz) the pulses are delayed by 40 ms each. The pulse itself consists of a single period of a sine with frequency $f_{pump} \approx 40$ MHz.

The voltage V_{GD} allows us to adjust the depth of the QD potential and thereby to tune the average number $\langle n \rangle = \sum_n n P_n$ of captured electrons [28]. Figure 3 shows P_n as measured by charge detection as a function of V_{GD}. The probabilities of charging the QD with up to 4 electrons are well resolved. For $n = 1$ the initialization accuracy reaches 99.1% for $V_{GD} \approx -192.5$ mV. The probability to charge the QD with 4 electrons with one initialization pulse approaches 80% for $V_{GD} \approx -168$ mV. We will analyze the V_{GD} dependence of P_n further below. In the following, a theoretical framework is established later allowing us to relate the measured distribution to the underlying capturing mechanisms.

Recent theoretical arguments [29] and experimental evidence [16] suggest that nonadiabatic quantum excitations in the source lead and in the dynamic QD, respectively, can be neglected for a sufficiently slow capture process. This warrants a Markovian approximation to the perturbative

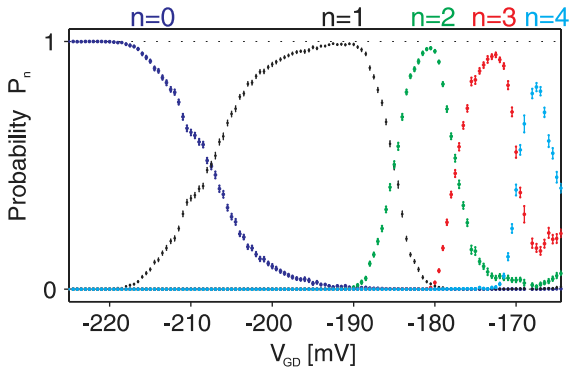

FIG. 3 (color online). Probabilities to capture $n = 0 \ldots 4$ electrons per cycle derived by counting as a function of V_{GD}. The error bars indicate the 95% confidence interval.

treatment of uncorrelated tunneling events [30,31] with time-dependent rates [26,32,33]. The "disequilibration" and eventual freezing of $P_n(t)$ can thus be described by a general master equation:

$$\dot{P}_n(t) = P_{n-1}(t)W^+_{n-1}(t) - P_n(t)W^-_n(t) + P_{n+1}(t)W^-_{n+1}(t) - P_n(t)W^+_n(t), \quad (1)$$

where $W^\pm_n$ are the instantaneous rates for adding (+) or removing (−) an electron to or from the QD, averaged over all degrees of freedom except n. Equation (1) holds for $n \geq 1$; $P_0(t)$ is deduced from normalization. We define $\mu_n(t)$ as

$$e^{\beta\mu_n(t)} \equiv W^-_n(t)/W^+_{n-1}(t), \quad (2)$$

with $\beta^{-1} \equiv kT$ being the product of temperature and Boltzmann's constant. If the time dependence of rates $W^\pm_n(t)$ is quasistatic, then Eq. (2) is the expression of thermodynamic detailed balance, $\mu_n = \Omega_n - \Omega_{n-1}$ is the electrochemical potential of a state with n electrons, and is equal to the differences in the thermodynamic potentials [31] $\Omega_n \equiv \mathcal{F}_n + E_n - nE_F$, where $\mathcal{F}_n$ is the canonical free energy of the internal degrees of freedom on the QD, E_n is the electrostatic interaction energy and $E_F \equiv 0$ is the Fermi level in the source lead. Defining the total rate for charge exchange in the $n \leftrightarrow n-1$ transition as $\Gamma_n(t) \equiv W^-_n(t) + W^+_{n-1}(t)$ allows us to write Eq. (1) in the form

$$\dot{P}_n(t) = -\Gamma_n[\bar{f}(\mu_n)P_n(t) - f(\mu_n)P_{n-1}(t)] + \Gamma_{n+1}[\bar{f}(\mu_{n+1})P_{n+1}(t) - f(\mu_{n+1})P_n(t)], \quad (3)$$

where $f(x) = 1/(1+e^{\beta x})$ is the Fermi distribution in the source and $\bar{f} \equiv 1 - f$.

We will now apply Eq. (3) to the decoupling process sketched in Fig. 2(a-i)–(a-ii). The end of the decoupling stage (ii) is characterized by $\Gamma_n(t_f) = 0$. The exact time dependencies of $\mu_n(t)$ and $\Gamma_n(t)$ between an initial time moment t_0 and t_f are impossible to predict without a more specific microscopic model for the QD. However, we can identify two relevant time moments for each transition $n-1 \leftrightarrow n$: one for the onset of backtunneling, t^b_n, and the other one for decoupling (detailed balance breakdown), t^c_n, described in Fig. 2(b). It shows schematically the evolution of Γ_n (blue) and μ_n (green) with time for the initialization process with two different values of V_{GD}. t^b_n is defined by the crossing of the Fermi level, $\mu_n(t^b_n) = 0$, while t^c_n is set by the average number of remaining tunneling events being of order one, $\int_{t^c_n}^{t_f} \Gamma_n(t)dt = 1$ (shaded area under the curve). Positive charging energies and the raising bottom of the confining potential well imply $t^b_{n+1} < t^b_n$ while in the relevant regime we expect the higher n states to be less stable, $\Gamma_{n+1}(t) > \Gamma_n(t)$ (at least for $t > t^b_n$) and therefore generally $t^c_{n+1} > t^c_n$. Sufficiently long equilibration before the decoupling implies that t^c_n is well defined for all n for which the Coulomb blockade holds. Fluctuations in the capture probability (i.e., P_n) will be strongest for n that have t^c_n and t^b_n close to each other [29].

We proceed by solving Eq. (3) for $P_n \equiv P_n(t_f)$ in two limits (thermal versus athermal) that correspond to opposing physical mechanisms of charge capture. We assume that initially the charge on the QD is equilibrated, corresponding to a grand canonical distribution, $P_n(t_0) \propto e^{-\beta\Omega_n(t_0)}$. As long as $\Gamma_n(t)$ remain sufficiently large, the solution $P_n(t)$ at $t > t_0$ closely follows the instantaneous equilibrium. This can be seen directly from Eq. (3): large Γ_n pin the terms in square brackets to zero and the evolving distribution of n obeys detailed balance adiabatically,

$$P_n(t) \approx e^{\beta\mu_{n+1}(t)}P_{n+1}(t). \quad (4)$$

In deriving the thermal limit we consider *sudden decoupling*, i.e., $\Gamma_{n+1}(t)$ dropping to 0 so fast that Eq. (4) must hold up to $t = t^c_{n+1}$, but once $t > t^c_{n+1}$ the right-hand side of Eq. (3) is effectively zero and $P_n(t)$ freezes (i.e., remains constant). With this sudden approximation, the asymptotic value $P_n = P_n(t^c_{n+1})$ is set by a "curtailed" grand canonical distribution that excludes already frozen charge states with $n' < n$ but is normalized over the remaining states with $n' \geq n$ that keep being connected until t^c_{n+2}. This gives $P_n = (1 - \sum_{m=0}^{n-1} P_m)\mathcal{Z}^{-1}_{n+1}$ or explicitly

$$P_n = \mathcal{Z}^{-1}_{n+1}\prod_{m=1}^{n}(1 - \mathcal{Z}^{-1}_m), \quad (5)$$

where $\mathcal{Z}_n \equiv 1 + \sum_{m=n}^{\infty}\prod_{l=n}^{m} e^{-\beta\mu_l(t^c_n)} = 1 + e^{-\beta\mu_n(t^c_n)}[1 + e^{-\beta\mu_{n+1}(t^c_n)}(1+\ldots)]$ includes the electrochemical potentials $\mu_{n'}$ of states $n' \geq n$ taken at the decoupling moment t^c_n of the state n. The assumption of well-pronounced Coulomb blockade implies that the addition energy, $\Delta\mu(t) \equiv \mu_n(t) - \mu_{n-1}(t)$ remains large compared to temperature. Thus there exists sufficiently large δ_T such that $\beta\Delta\mu(t) \geq \delta_T$ for all relevant n and t. For $\delta_T \gg 1$, a further approximation, $\mathcal{Z}_n \approx 1 + e^{-\beta\mu_n(t^c_n)}$, results in at most $e^{-\delta_T}$ relative error for each P_n, leading to a simple expression for the low-dispersion limit of the sudden decoupling mechanism,

$$P_n = \bar{f}[\mu_{n+1}(t^c_{n+1})]\prod_{m=1}^{n} f[\mu_m(t^c_m)]. \quad (6)$$

The distribution (6) is determined by a set of dimensionless numbers $\tilde{\mu}_n \equiv \beta\mu_n(t^c_n)$ and is narrowly dispersed if $\ldots \gg \tilde{\mu}_{m+1} \gg \tilde{\mu}_m \gg \ldots$.

Now we consider the athermal limit. At sufficiently low temperatures the time scale for $f[\mu_n(t)]$ switching between loading (≈ 1) and unloading (≈ 0) may become much shorter than the time scale of reducing $\Gamma_n(t)$. Assessing this gradual decoupling limit amounts to replacing the Fermi functions in Eq. (3) by sharp steps, $f(\mu_n) \to \Theta(t - t^b_n)$. Starting with a sharp initial equilibrium free of thermal fluctuations, $P_n(t_0) = \delta_{n,N}$ with $t^{N+1}_b < t_0 < t^N_b$, the system of equations (3) is reduced to a set of decay cascade equations:

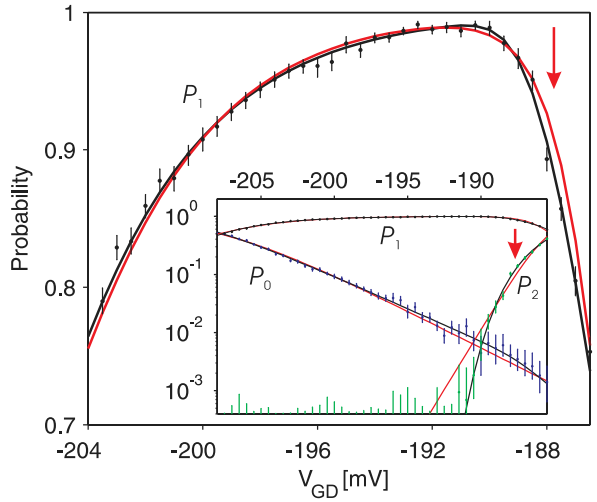

FIG. 4 (color online). Measured P_1 (points) as function of V_{GD}, compared to theoretical fits to thermal and athermal limit (red or gray and black solid lines, respectively). The error bars indicate 95% confidence intervals. The uncertainty in V_{GD} is smaller than the linewidth of the error bars. The blue, black and green data points correspond to P_0, P_1, and P_2, as labeled, respectively, shown on a logarithmic scale in the inset.

$$\dot{P}_n(t) = \begin{cases} 0, & t < t^b_{n+1}, \\ \Gamma_{n+1}P_{n+1}(t), & t^b_{n+1} < t < t^b_n, \\ -\Gamma_n P_n(t) + \Gamma_{n+1}P_{n+1}(t), & t^b_n < t. \end{cases} \quad (7)$$

These equations generalize the decay cascade model [13] to distinct t^b_n's. One can show that a universal solution to Eq. (7) independent of the specific shape of $\Gamma_n(t)$'s time dependence [13],

$$P_n = e^{-X_n} \prod_{j=n+1}^{N} (1 - e^{-X_j}), \quad (8)$$

remains valid in the limit of $\ldots \gg X_{j+1} \gg X_j \gg \ldots$ with appropriately generalized integrated decay rates, $X_n \equiv \int_{t^b_n}^{t_f} \Gamma_n(t)dt \overset{T\to 0}{=} \int_{t_0}^{t_f} W^-_n(t)dt$.

Distinguishing the two theoretical limits (6) and (8) in a counting experiment requires information on the dependence of $\tilde{\mu}_n$ and X_n on the control parameters such as V_{GD} and/or f_{pump}. We assume that $V_{GS}(t)$ and V_{GD} affect $\mu_n(t)$ linearly and $W^-(t)$ exponentially (typical for decay rates controlled by an energy barrier); see Fig. 2(b). Following the definitions of X_n and $\tilde{\mu}_n$, this assumption leads to the following parametrization:

$$\tilde{\mu}_n = -\alpha_{\mu,n}V_{GD} + \Delta_{\mu,n}, \quad (9a)$$

$$\ln X_n = -\alpha_{X,n}V_{GD} + \Delta_{X,n}. \quad (9b)$$

Although the operation frequency was not varied in our measurements, we note that changing $f_{pump} \to xf_{pump}$ is equivalent to reducing all $W^{\pm}_n(t)$ by a factor of x while leaving $\mu_n(t)$ intact, as long as the time dependencies remain parametric. Thus we expect $\Delta_{X,n}(f_{pump}) = -\ln f_{pump} + \text{const}$ [34]. This is consistent with an experimental study of the capture probability as function of driving rate [11].

Our measurement results for P_n as a function of V_{GD} in the region of single electron capture ($P_1 \approx 1$) are compared to the thermal [Eqs. (6) and (9a)] and athermal [Eqs. (8) and (9b)] distributions in Fig. 4. We use $\{\alpha_{\mu,n}, \Delta_{\mu,n}\}$ and $\{\alpha_{X,n}, \Delta_{X,n}\}$ as fit parameters for the respective models; the maximal likelihood values are given in Table I. Only $0 \leftrightarrow 1$ and $1 \leftrightarrow 2$ transitions have been considered since P_n with $n > 2$ do not contribute for $V_{GD} < -186$ mV (see Fig. 3). The error bars on the data indicate 95% confidence intervals for estimating probability from the binomial statistics of direct counting [27,35]. Measurement data deviate from the thermal limit (red solid line) beyond confidence interval for voltages $V_{GD} > -190$ mV for P_1 on linear scale (marked by red arrow). Note also that the uncertainties for the model parameters turn out larger for the thermal model (see Table I). Even stronger deviations can be observed for P_2 on the logarithmic scale. Here the thermal model predicts a linear characteristic, while the apparent nonlinearity is reproduced well by the athermal limit. Thus, our measured distribution is consistent with the generalized decay cascade model in the low-noise limit.

The generalized decay cascade limit implies that lowering the lead temperature will not increase the initialization precision, which has indeed been found in surface acoustic wave driven devices [36]. This feature alone would, however, not suffice to exclude the thermal distribution as in the past this saturation has been related to rf heating induced by the modulation [36,37]. Our results indicate a path for further improvements for dynamic QD initialization: it may be achieved by increasing the separation of decay steps (X_n/X_{n-1}) either by a large decay rate ratio [$\Gamma_n(t)/\Gamma_{n-1}(t)$] [13] or large energy separation $\Delta\mu$, in which case $\Gamma_n(t^b_n)/\Gamma_{n-1}(t^b_{n-1})$ can be large even if $\Gamma_n(t) \approx \Gamma_{n-1}(t)$, due to the difference in t^b_{n-1} and t^b_n. Alternatively, devices with reduced coupling between barrier and plunger may benefit from the *thermal* limit at which lowering the temperature will further enhance the initialization precision. This regime may be reached by adding compensation pulses to V_{GD} during the transition (i) → (ii) in Fig. 2.

TABLE I. Best fit parameters.

	$\alpha_{\mu/X,1}/\text{mV}^{-1}$	$\alpha_{\mu/X,2}/\text{mV}^{-1}$	$\Delta_{\mu/X,1}$	$\Delta_{\mu/X,2}$
Thermal	-0.293 ± 0.003	-0.983 ± 0.023	-60.8 ± 0.6	-182.1 ± 4.2
Athermal	0.261 ± 0.003	0.385 ± 0.009	-54.5 ± 0.6	-71.5 ± 1.6

Within the decay-cascade limit the effect of frequency on precision depends on the coupling coefficients $\alpha_{X,n}$ and is hence device specific. Albeit the precision may improve by increasing f_{pump} over a limited range, at even higher frequencies more degrees of freedom than just the total charge are expected to go out of equilibrium [16,29], engaging new capture mechanisms beyond the scope of our quasiclassical Markovian description. However, the demonstrated experimental counting technique is applicable over a large dynamical range, and thus will be an important tool for exploration of the high-speed frontier in nonequilibrium single-electron manipulation.

This work has been supported by the DFG and within the Joint Research Project "Quantum Ampere" (JRP SIB07) within the European Metrology Research Programme (EMRP). The EMRP is jointly funded by the EMRP participating countries within EURAMET and the European Union. V. K., J. T., and P. N. have been supported by ESF Project No. 2009/0216/1DP/1.1.1.2.0/09/APIA/VIAA/044.

*bernd.kaestner@ptb.de

[1] D. V. Averin and K. K. Likharev, *Mesoscopic Phenomena in Solids* (Elsevier, Amsterdam, 1991), p. 173.
[2] C. H. W. Barnes, J. M. Shilton, and A. M. Robinson, Phys. Rev. B **62**, 8410 (2000).
[3] G. Gumbs, D. Huang, M. D. Blumenthal, S. J. Wright, M. Pepper, and Y. Abranyos, Semicond. Sci. Technol. **24**, 115001 (2009).
[4] S. Amakawa, K. Tsukagoshi, K. Nakazato, H. Mizuta, and B. W. Alphenaar, *Single-Electron Logic Based on Multiple-Tunnel Junctions* edited by, H. Nakashima, Mesoscopic Tunneling Devices (Research Signpost, Kerala, 2004), pp. 71–104.
[5] Y. Ono, A. Fujiwara, K. Nishiguchi, H. Inokawa, and Y. Takahashi, J. Appl. Phys. **97**, 031101 (2005).
[6] J. M. Shilton, V. I. Talyanskii, M. Pepper, D. A. Ritchie, J. E. F. Frost, C. J. B. Ford, C. G. Smith, and G. A. C. Jones, J. Phys. Condens. Matter **8**, L531 (1996).
[7] M. D. Blumenthal, B. Kaestner, L. Li, S. Giblin, T. J. B. M. Janssen, M. Pepper, D. Anderson, G. Jones, and D. A. Ritchie, Nat. Phys. **3**, 343 (2007).
[8] J. P. Pekola, O.-P. Saira, V. F. Maisi, A. Kemppinen, M. Möttönen, Y. A. Pashkir, and D. V. Averin, arXiv:1208.4030v2.
[9] I. M. Mills, P. J. Mohr, T. J. Quinn, B. N. Taylor, and E. R. Williams, Metrologia **43**, 227 (2006).
[10] CCEM Working Group on the SI, Report No. CCEM/09-05, 2009.
[11] A. Fujiwara, K. Nishiguchi, and Y. Ono, Appl. Phys. Lett. **92**, 042102 (2008).
[12] B. Kaestner, C. Leicht, V. Kashcheyevs, K. Pierz, U. Siegner, and H. W. Schumacher, Appl. Phys. Lett. **94**, 012106 (2009).
[13] V. Kashcheyevs and B. Kaestner, Phys. Rev. Lett. **104**, 186805 (2010).
[14] C. Liu and Q. Niu, Phys. Rev. B **47**, 13 031 (1993).
[15] K. Flensberg, Q. Niu, and M. Pustilnik, Phys. Rev. B **60**, R16291 (1999).
[16] M. Kataoka, J. D. Fletcher, P. See, S. P. Giblin, T. J. B. M. Janssen, J. P. Griffiths, G. A. C. Jones, I. Farrer, and D. A. Ritchie, Phys. Rev. Lett. **106**, 126801 (2011).
[17] S. P. Giblin, S. J. Wright, J. D. Fletcher, M. Kataoka, M. Pepper, T. J. B. M. Janssen, D. A. Ritchie, C. A. Nicoll, D. Anderson, and G. A. C. Jones, New J. Phys. **12**, 073013 (2010).
[18] F. Hohls, A. C. Welker, C. Leicht, L. Fricke, B. Kaestner, P. Mirovsky, A. Müller, K. Pierz, U. Siegner, and H. W. Schumacher, Phys. Rev. Lett. **109**, 056802 (2012).
[19] S. P. Giblin, M. Kataoka, J. D. Fletcher, P. See, T. J. B. M. Janssen, J. P. Griffths, G. A. C. Jones, I. Farrer, and D. A. Ritchie, Nat. Commun. **3**, 930 (2012).
[20] J. D. Fletcher, M. Kataoka, S. P. Giblin, S. Park, H. Sim, P. See, D. A. Ritchie, J. P. Griffiths, G. A. C. Jones, H. E. Beere, and T. J. B. M. Janssen, Phys. Rev. B **86**, 155311 (2012).
[21] G. Yamahata, K. Nishiguchi, and A. Fujiwara, Appl. Phys. Lett. **98**, 222104 (2011).
[22] A. M. Robinson and V. I. Talyanskii, Phys. Rev. Lett. **95**, 247202 (2005).
[23] N. Maire, F. Hohls, B. Kaestner, K. Pierz, H. W. Schumacher, and R. J. Haug, Appl. Phys. Lett. **92**, 082112 (2008).
[24] E. Bocquillon, F. D. Parmentier, C. Grenier, J.-M. Berroir, P. Degiovanni, D. C. Glattli, B. Plaçais, A. Cavanna, Y. Jin, and G. Fève, Phys. Rev. Lett. **108**, 196803 (2012).
[25] M. Kataoka, R. J. Schneble, A. L. Thorn, C. H. W. Barnes, C. J. B. Ford, D. Anderson, G. A. C. Jones, I. Farrer, D. A. Ritchie, and M. Pepper, Phys. Rev. Lett. **98**, 046801 (2007).
[26] B. Kaestner, V. Kashcheyevs, S. Amakawa, M. D. Blumenthal, L. Li, T. J. B. M. Janssen, G. Hein, K. Pierz, T. Weimann, U. Siegner, and H. W. Schumacher, Phys. Rev. B **77**, 153301 (2008).
[27] See Supplemental Material at http://link.aps.org/supplemental/10.1103/PhysRevLett.110.126803 for the extraction of probabilities P_n from the raw counting data.
[28] B. Kaestner, V. Kashcheyevs, G. Hein, K. Pierz, U. Siegner, and H. W. Schumacher, Appl. Phys. Lett. **92**, 192106 (2008).
[29] V. Kashcheyevs and J. Timoshenko, Phys. Rev. Lett. **109**, 216801 (2012).
[30] D. V. Averin, A. N. Korotkov, and K. K. Likharev, Phys. Rev. B **44**, 6199 (1991).
[31] C. W. J. Beenakker, Phys. Rev. B **44**, 1646 (1991).
[32] F. Pistolesi, Phys. Rev. B **69**, 245409 (2004).
[33] F. Battista and P. Samuelsson, Phys. Rev. B **83**, 125324 (2011).
[34] Note that for t_n^c to be well defined and the sudden approximation leading to Eq. (6) to be applicable, $\Gamma_n(t)$ must change many orders of magnitude within the time interval $kT/\dot{\mu}_n$ around t_n^c; thus, we expect $\tilde{\mu}_n$ and, in particular, $\Delta_{\mu,n}$ to be insensitive to frequency within the approximations made.
[35] W. H. Press, S. A. Teukolsky, and W. T. Vetterling, *Numerical Recipes, The Art of Scientific Computing* (Cambridge University Press, Cambridge, England, 2007), 3rd ed.
[36] J. T. Janssen and A. Hartland, IEEE Trans. Instrum. Meas. **50**, 227 (2001).
[37] P. Utko, P. E. Lindelof, and K. Gloos, Appl. Phys. Lett. **88**, 202113 (2006).